Available online at www.sciencedirect.com
ScienceDirect
International Journal of Solids and Structures 44 (2007) 4492–4504
INTERNATIONAL JOURNAL OF SOLIDS and STRUCTURES
www.elsevier.com/locate/ijsolstr

Small scale, grain size and substrate effects in nano-indentation experiment of film–substrate systems

S.H. Chen *, L. Liu, T.C. Wang

LNM, Institute of Mechanics, Chinese Academy of Sciences, No. 15, BeiSiHuan Xilu, Beijing 100080, China

Received 3 July 2006; received in revised form 13 October 2006
Available online 1 December 2006

Abstract

The mechanical properties of film–substrate systems have been investigated through nano-indentation experiments in our former paper (Chen, S.H., Liu, L., Wang, T.C., 2005. Investigation of the mechanical properties of thin films by nano-indentation, considering the effects of thickness and different coating–substrate combinations. Surf. Coat. Technol., 191, 25–32), in which Al–Glass with three different film thicknesses are adopted and it is found that the relation between the hardness H and normalized indentation depth h/t, where t denotes the film thickness, exhibits three different regimes: (i) the hardness decreases obviously with increasing indentation depth; (ii) then, the hardness keeps an almost constant value in the range of 0.1–0.7 of the normalized indentation depth h/t; (iii) after that, the hardness increases with increasing indentation depth. In this paper, the indentation image is further investigated and finite element method is used to analyze the nano-indentation phenomena with both classical plasticity and strain gradient plasticity theories. Not only the case with an ideal sharp indenter tip but also that with a round one is considered in both theories. Finally, we find that the classical plasticity theory can not predict the experimental results, even considering the indenter tip curvature. However, the strain gradient plasticity theory can describe the experimental data very well not only at a shallow indentation depth but also at a deep depth. Strain gradient and substrate effects are proved to coexist in film–substrate nano-indentation experiments.

Keywords: Nano-indentation hardness; Film–substrate system; Classical plasticity theory; Strain gradient plasticity theory; Indenter tip curvature; FEM

1. Introduction

Micro and nano-indentation hardness experiments are widely used to measure the plastic flow resistance of materials. It has been shown repeatedly that the hardness of metallic materials displays a strong size effect with conical or pyramidal indenters. The measured indentation hardness can increase by a factor of two or three as the indentation depth decreases into micrometers, even to tens to hundreds of nanometers (e.g., Nix, 1989; Oliver and Pharr, 1992; Stelmashenko et al., 1993; Ma and Clarke, 1995; Poole et al., 1996; McElhaney

* Corresponding author. Tel.: +86 10 62615517; fax: +86 10 62561284.
E-mail address: chenshaohua72@hotmail.com (S.H. Chen).

0020-7683/$ - see front matter
doi:10.1016/j.ijsolstr.2006.11.033

et al., 1998; Nix and Gao, 1998; Suresh et al., 1999; Xue et al., 2002; Huang et al., 2004; Swaddiwudhipong et al., 2005, 2006a,b). The indentation size effect has also been investigated using spherical indenters (e.g., Swadener et al., 2001, 2002; Wei and Hutchinson, 2003b; Qu et al., 2004, 2006), where the indentation hardness depends on not only the indentation depth but also the indenter radius. Size effects have also been found in other micron and sub-micron scale experiments. Experimental work on particle-reinforced metal matrix composites has revealed that a substantial increase in the macroscopic flow stress can be achieved by decreasing the particle size while keeping the volume fraction unchanged (Lloyd, 1994). Fleck et al. (1994) reported that the strength of thin copper wires increases with decreasing diameter of thin wires in micro-torsion. The facts of the strength increasing with decreasing thickness of thin beams in micro-bending test are found by Stolken and Evans (1998), Shrotriya et al. (2003) and Haque and Saif (2003). Thermo-mechanical fatigue has relation with the spatial strain gradient effects too (Pucha et al., 2004).

Conventional plasticity theory can not explain the above size-dependent material behavior at the small scales because no intrinsic material lengths are involved. The size-dependent behavior has been attributed to geometrically necessary dislocations associated with non-uniform plastic deformation in small volumes (e.g., Gao et al., 1999; Huang et al., 2000a; Voyiadjis and Abu Al-Rub, 2005).

Based on the concept of geometrically necessary dislocations, strain gradient theories have been developed. These theories believed that the flow stress not only relies on strain in particular point as in conventional plasticity theory, moreover also relies on the strain gradient at that point. Generally, the gradient plasticity theories to model size effects can be divided into two groups. The first one involves higher-order stresses and higher-order boundary conditions, such as the CS and SG theories (e.g., Fleck and Hutchinson, 1993, 1997; Wei and Hutchinson, 1997, 2003b; Gurtin, 2002, 2003) and MSG theory (Gao et al., 1999; Huang et al., 2000a; Hwang et al., 2002). The second group does not involve the higher-order stresses and the equilibrium equations remain the same as those of classical theory (e.g., Acharya and Bassani, 2000; Bassani, 2001; Chen and Wang, 2000, 2001, 2002a,b; Gao and Huang, 2001; Abu Al-Rub and Voyiadjis, 2004, 2006; Hu and Huang, 2004; Liu and Hu, 2005; Voyiadjis and Abu Al-Rub, 2005). Huang et al. (2000a) showed that the higher-order stresses have little or essentially no effect on the predictions of size effects in micro-torsion, micro-bending, micro-indentation, crack tip, void growth and MSG theory was modified by Huang et al. (2004) such that it does not include the higher-order stresses and preserves the structure of conventional plasticity theory, which becomes very convenient for application. All these strain gradient theories have been used to analyze the experimental phenomena and to some extent most theoretical and simulation results are consistent with experimental data. Besides the strain gradient theories, other models to study the size effects have been investigated, such as a model based on a surface work and plastic volume work concept (Horstemeyer et al., 2001; Gerberich et al., 2002) and a model considering the surface and interface energy (Duan et al., 2005).

For the indentation problem of film–substrate system, the results are influenced strongly by substrates, which result in extreme difficulty to measure the mechanical properties of film material. The commonly used method is to limit the depth of impression below 10% film thickness, but this method is only available for the film thickness larger than 1 μm, and cannot give accurate results for the film with very small thickness such as nanometer or sub-micro scales. Wei et al. (2003c) considered the effect from both the crystal grain size and the grain shape distribution in the thin film–substrate system. Recently Saha and Nix (2002) used a method called constant Young's modulus assumption and analyzed the hardness and elastic moduli of both soft films on hard substrates and hard films on soft substrates. Saha et al. (2001) also used MSG theory (Gao et al., 1999) to investigate the strain gradient effect in nano-indentation of film–substrate systems and found that the MSG theory could describe the new phenomena well. Chen et al. (2005) carried out nano-indentation experiments on kinds of film–substrate systems and the experimental results were successfully explained (Chen et al., 2004a) by the strain gradient theory proposed in Chen and Wang (2000, 2001, 2002a,b). Using discrete dislocation simulation of nano-indentation, Kreuzer and Pippan (2005) found that the hardness values vs. the number of contact elements (size of the indentation) illustrates the same typical trend (decreasing hardness with increasing indentation depth, followed by an increase of the hardness when the indenter feels the presence of the substrate) as that in Chen et al. (2005), which verifies the basis of geometric necessary dislocation in strain gradient plasticity theories.

As we know that the effects of spherical tip are different from that of the conical or pyramidal indenter (Xue et al., 2002; Wei and Hutchinson, 2003b; Qu et al., 2006). In real experiments the conical or pyramidal indenter tip is not usually ideal sharp, which possesses a curvature. What effect does the tip round has? Numerical

simulations of the nano-indentation on film–substrate systems often take empirical formula to obtain the film parameters, such as the yield stress, power-law hardening exponent (e.g., Saha et al., 2001; Chen et al., 2004a). How can we obtain the film parameters from the experimental data directly? In the present paper, nano-indentation experimental results on Al–glass systems with different film thicknesses have been analyzed and simulated. The film material parameters, such as yield stress, the power-law hardening exponent and intrinsic length in strain gradient theory, can be obtained through fitting the experimental load–depth curve with finite element calculation. Both the classical plasticity and strain gradient plasticity theories are adopted. The influence of indenter tip curvature on the measured hardness is also considered. Finally, it shows that the strain gradient plasticity theory can describe the complex relation between the hardness and the indentation depth very well, but the results predicted by the classical plasticity theory are much smaller than the experimental data. Furthermore, in contrast to the case with an ideal sharp indenter tip, a round indenter tip will reduce the experimental hardness during the shallow indentation depth.

2. Experimental results

Details about the nano-indentation experiments on film–substrate systems can be found in Chen et al. (2005), here we only give some brief information and results for Al–glass systems.

In the experiment, one of the films is aluminum, which is deposited onto glass substrate by sputtering with three nominal thicknesses, 52, 245 and 851 nm. The mechanical properties of the substrates and films are firstly characterized using a Nano Indenter XP II equipped with a standard Berkovich indenter. Continuous stiffness method (CSM) is used in all experiments. The indentations have been done with a constant nominal strain rate ($\dot{h}/h$) 0.05 s^{-1}. Five indentations are chosen in each sample and the results presented are the average of these five indentations. During the experiments, hardness and Young's modulus are measured using Oliver and Pharr (1992) method (O&P method). As we know that O&P method has become a standard method in nano-indentation instruments, but it should be noticed that Oliver and Pharr method is developed only for monolithic materials and the modified contact area function is established only for sink-in phenomenon. From indentation images of scanning electron microscopy (SEM) as shown in Fig. 1 (a), we find that pile-up happens at the edge of indenter, which will result in an overestimation of hardness and elastic modulus and an underestimation of the contact area. In order to avoid the influence of the contact area calculation, we have adopted Joslin and Oliver (1990) method and Constant Young's modulus assumption (CYMA) to analyze the experimental data and obtained the true hardness variation (Chen et al., 2005) for Al–glass because the Young's modulus of Al film is very close to that of glass substrate.

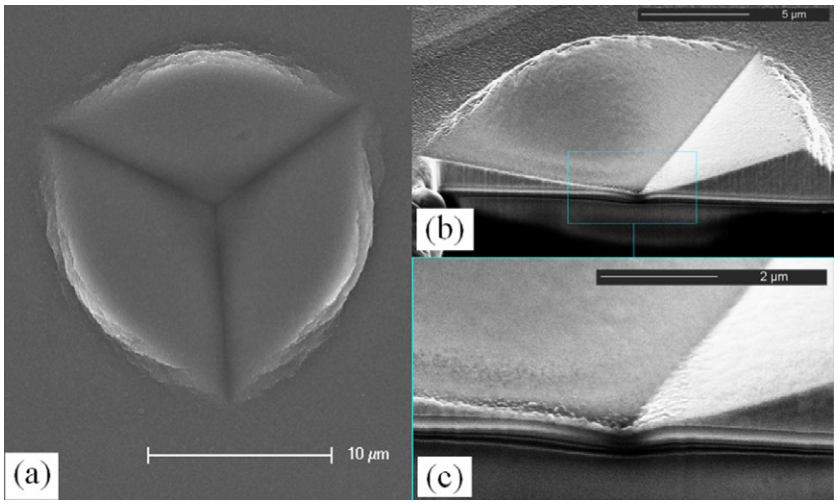

Fig. 1. (a) Indentation SEM image of Al film on glass substrate. The light area denotes pile-up. (b) SEM cross-section micrograph of a Berkovich indentation. (c) Amplified picture of the cross-section, which illustrates the strain gradient between the diamond indenter and the hard glass substrate.

Nano-indentation hardness of Al–glass with different film thicknesses versus the normalized indentation depth h/t is shown in Fig. 2. One can see that at initial stage, the hardness decreases with increasing indentation depth, which is also expected for bulk metallic materials. As the indentation depth increases, the indentation hardness keeps almost a constant in the second stage. In the third stage, it increases with an increasing indentation depth, which is impossible for single bulk material. Comparing the indentation hardness of film–substrate systems with different film thicknesses, one can find that the smaller the film thickness, the larger the hardness is. The constant values of hardness for systems with different film thicknesses are 0.9 GPa for 851 nm film, 1.1 GPa for 245 nm film and 1.8 GPa for 52 nm film, respectively.

With the help of focus ion beam (FIB) and SEM, the cross-section deformations of indented samples are shown in Fig. 1(b) and (c). One can see that the cross-section of Al–glass system after unloading clearly shows the compression of the film thickness between the indenter and the hard glass substrate. Motivated by Hwang et al. (2002), in which it is found that the finite deformation effect is not very significant for modeling indentation experiments, small deformation theory will be used in this paper.

3. Brief review of strain gradient plasticity theory

Strain gradient plasticity theory proposed by Chen and Wang (2000, 2001, 2002a,b) will be used to analyze the above experimental results. It preserves the same equilibrium equations as those of classical theory and involves no higher-order stresses or higher-order strain rates. The key features of the theory are that the rotation gradient influences the material behavior through the interaction between the Cauchy stress and couple stress, while the stretch gradient explicitly enters the constitutive relations through the instantaneously tangential modulus. The tangential hardening modulus is influenced by not only the generalized effective strain but also the effective stretch gradient.

The strain tensor ε_{ij} and the stretch gradient tensor η_{ijk} (Smyshlyaev and Fleck, 1996) are both related to the displacement u_i by

$$\varepsilon_{ij} = \frac{1}{2}(u_{i,j} + u_{j,i}), \quad \eta_{ijk} = u_{k,ij}. \tag{1}$$

The relationship between the rotation gradient χ_{ij} and the independent micro-rotation vector ω_i is

$$\chi_{ij} = \omega_{i,j}. \tag{2}$$

The effective strain ε_e, effective rotation gradient χ_e and effective stretch gradient η_1 are defined as

$$\varepsilon_e = \sqrt{2\varepsilon'_{ij}\varepsilon'_{ij}/3} \quad \chi_e = \sqrt{2\chi'_{ij}\chi'_{ij}/3} \quad \eta_1 = \sqrt{\eta^{(1)}_{ijk}\eta^{(1)}_{ijk}}, \tag{3}$$

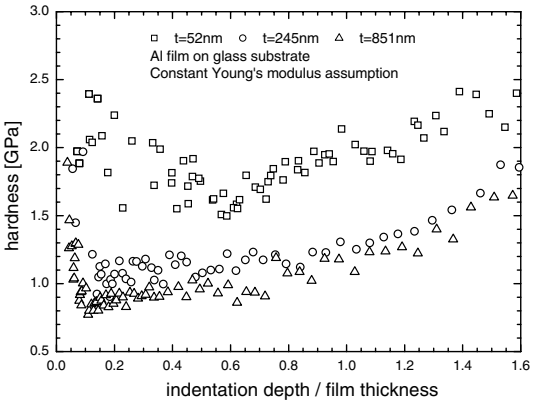

Fig. 2. Experimental results of hardness of Al–glass obtained by Joslin and Oliver (1990) method and constant Young's modulus assumption versus the normalized indentation depth by film thickness.

where ε'_{ij} and χ'_{ij} are the deviatoric parts and the definition of $\eta^{(1)}_{ijk}$ can be found in Smyshlyaev and Fleck (1996) and the formula for numerical calculation of η_1 can be found in Chen and Wang (2002b).

The constitutive relations are as follows

$$\begin{aligned}\sigma_{ij} &= \frac{2\Sigma_e}{3E_e}\varepsilon'_{ij} + K\varepsilon_m\delta_{ij},\\ m_{ij} &= \frac{2\Sigma_e}{3E_e}l_{cs}^2\chi'_{ij} + K_1 l_{cs}^2\chi_m\delta_{ij},\end{aligned} \tag{4}$$

where

$$\begin{cases} E_e^2 = \varepsilon_e^2 + l_{cs}^2\chi_e^2, & \Sigma_e^2 = \sigma_e^2 + l_{cs}^{-2}m_e^2,\\ \sigma_e^2 = \frac{3}{2}s_{ij}\ s_{ij}, & m_e^2 = \frac{3}{2}m'_{ij}\ m'_{ij}, \end{cases} \tag{5}$$

E_e is called the generalized effective strain and Σ_e is the work conjugate of E_e; l_{cs} is an intrinsic material length, which reflects the effect of the rotation gradient; K is the volumetric modulus and K_1 is the bend-torsion volumetric modulus.

The effect of the stretch gradient on material behaviors is introduced through the following incremental hardening law

$$\begin{cases} \dot{\Sigma}_e = A'(E_e)\sqrt{1+\frac{l\eta_1}{E_e}}\cdot\dot{E}_e = B(E_e, l\eta_1)\dot{E}_e, & \Sigma_e \geqslant \sigma_Y,\\ \dot{\Sigma}_e = 3\mu\dot{E}_e, & \Sigma_e < \sigma_Y, \end{cases} \tag{6}$$

where $B(E_e, l\eta_1)$ is a new hardening function including the effective stretch gradient; l is the second intrinsic material length associated with the stretch gradient; μ is the shear modulus and σ_Y is the yield stress.

On each incremental step in finite element calculation, both the effective strain ε_e and the effective stretch gradient η_1 can be obtained from the updated displacement fields; the effective rotation gradient χ_e can be obtained from the updated rotation fields. Hence η_1 is only a given parameter in Eq. (6) and it does not invoke higher-order stress or higher-order strain rates. When the stretch gradient is considered, the constitutive relations must be in an incremental form according to the incremental hardening law (6). From Eqs. (4) and (5), we obtain

$$\begin{cases} \dot{\sigma}_{ij} = 2\mu\dot{\varepsilon}'_{ij} + K\dot{\varepsilon}_m\delta_{ij}\\ \dot{m}_{ij} = 2\mu l_{cs}^2\ \dot{\chi}'_{ij} + K_1 l_{cs}^2\ \dot{\chi}_m\ \delta_{ij} \end{cases}, \quad \Sigma_e < \sigma_Y \tag{7}$$

$$\begin{cases} \dot{\sigma}_{ij} = \frac{2\Sigma_e}{3E_e}\dot{\varepsilon}'_{ij} + \frac{2\dot{\Sigma}_e}{3E_e}\varepsilon'_{ij} - \frac{2\Sigma_e}{3E_e^2}\varepsilon'_{ij}\dot{E}_e + K\dot{\varepsilon}_m\delta_{ij}\\ \dot{m}_{ij} = \frac{2\Sigma_e}{3E_e}l_{cs}^2\ \dot{\chi}'_{ij} + \frac{2\dot{\Sigma}_e}{3E_e}l_{cs}^2\ \dot{\chi}'_{ij} - \frac{2\Sigma_e}{3E_e^2}l_{cs}^2\ \chi'_{ij}\dot{E}_e + K_1 l_{cs}^2\ \dot{\chi}_m\delta_{ij} \end{cases}, \quad \Sigma_e \geqslant \sigma_Y \tag{8}$$

The above strain gradient theory has been successfully used to explain the size effects in thin-wire torsion (Chen and Wang, 2000, 2001, 2002a), thin-beam bending (Chen and Wang, 2000, 2001, 2002a), micro-indentation (Chen et al., 2004b), particle-reinforced metal matrix composites (Chen and Wang, 2002c) and the cleavage fracture near the crack tip (Chen and Wang, 2002b,d). It has also been used to analyze the small scale effects in film–substrate (Chen et al., 2004a), in which the parameters of films are obtained using empirical formula and only the ideal sharp indenter tip is considered.

4. Finite element method simulation

4.1. Calculation model

In order to consider the strain gradient, a second-order element should be used, such as eight-node or nine-node elements. The results obtained from eight-node elements have been found very close to that obtained from nine-node elements (Chen and Wang, 2002b). This kind of element is only suitable for solids with vanishing higher-order stress traction on the surface. For example, the element works very well in the fracture

analysis of strain gradient plasticity (Chen and Wang, 2002b,c; Wei and Hutchinson, 1997), where the higher-order stress tractions vanish on the crack face and on the remote boundary. This element also works well in the study of micro-indentation experiments (Huang et al., 2000b) because the higher-order stress tractions are zero on the indented surface. Since the strain gradient theory proposed by Chen and Wang (2000, 2001, 2002a,b) does not include higher-order stress or higher-order stress tractions, it will work well in the present study as discussed in the next section.

The scheme of conical indenter is shown in Fig. 3 with a half-angle $\varphi = 70.32°$, which gives the same cross-sectional area as that of Berkovich indenter used in the experiments at the same indentation depth. Axial symmetric calculation model is chosen and the finite element meshes are shown in Fig. 4, in which there are 545 elements and 1746 nodes. For a non-ideal indenter, as shown in Fig. 3, the relation of contact depth, δ, and contact radius, r, can be expressed as

$$\begin{cases} \delta(r) = R - (R^2 - r^2)^{1/2}, & 0 \leqslant r \leqslant r_0, \\ \delta(r) = \frac{r}{\tan\varphi} - \xi, & r_0 < r \leqslant a, \end{cases} \tag{9}$$

where R is the tip radius of the indenter, ξ is the blunting distance, r_0 is the contact radius of the blunt indenter and a represents the largest contact radius at the contact edge, $r_0 = R \cdot \cos\varphi$ and $\xi = R/\sin\varphi - R$. Moreover, the indenter is also assumed to be frictionless such that there is no sticking between the indenter and the indented materials.

The boundary conditions in the present model are described as follows,

(1) Along the symmetric axis ($r = 0$), the displacement $u_r(0, z)$ is zero, where (r, z) is cylindrical coordinate system.
(2) The upper and side surfaces of the indented body are traction-free except the pressure produced by the indenter. The displacement u_z at the bottom of the indented body is assumed to be zero.
(3) For a frictionless indenter, the materials in the contact region ($0 \leqslant r \leqslant a$) can slide up and down freely on the surface of the indenter. For an ideal indenter, we have

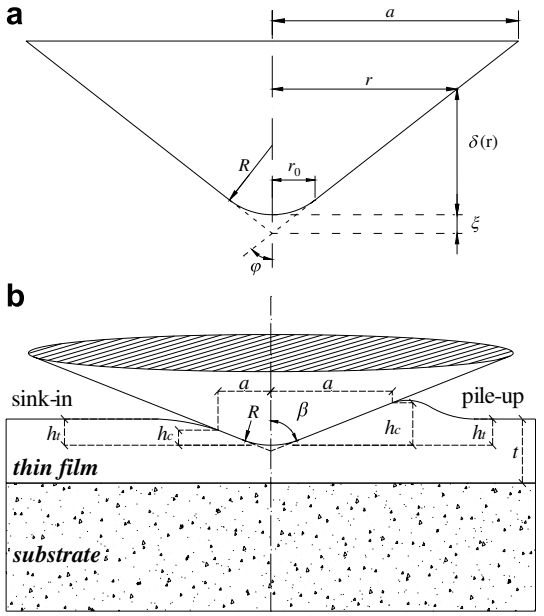

Fig. 3. (a) A spherically truncated conical indenter. (b) Schematic illustration of sink-in or pile-up in indentation. The total depth of indentation is denoted as h_t, the contact depth is h_c and the contact radius is a.

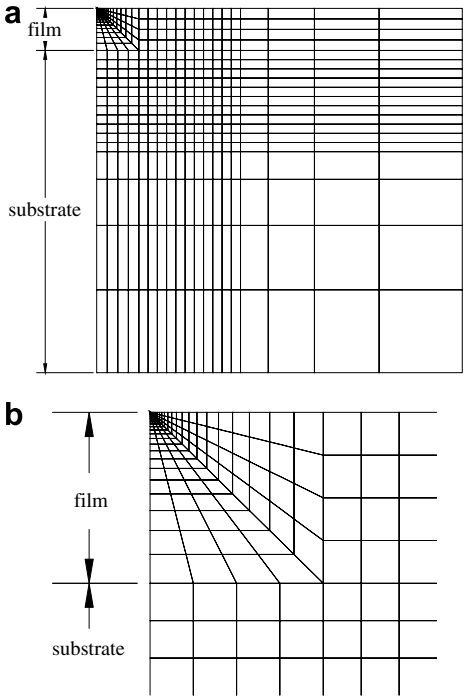

Fig. 4. (a) Finite element meshes for film–substrate model. (b) Locally amplified sketch map.

$$u_z(r) = \frac{r-a}{\tan\varphi}, \quad 0 \leqslant r \leqslant a. \tag{10}$$

For a spherically truncated conical indenter with tip radius R, there are

$$\begin{cases} u_z(r) = -\delta(a) + R - (R^2 - r^2)^{1/2}, & 0 \leqslant r \leqslant r_0, \\ u_z(r) = -\delta(a) - \xi + \frac{r}{\tan\varphi}, & r_0 < r \leqslant a. \end{cases} \tag{11}$$

(4) Other surfaces are tractions free.

In the present model, the contact between the indenter and the specimen is simulated by assuming a contact radius a first, then the indentation depth, h_t, which is defined as the depth where the normal stress between the indenter and the specimen vanishes at the edge of the contact region, i.e., $t_z|_{r=a} = 0$, can be found by iteration as shown in Fig. 3(b). The real contact depth, h_c, can be obtained as $h_c = a/\tan\varphi$ for ideal indenter and $h_c = a/\tan\varphi - \xi$ for round tip case.

The total load P is the sum of nodal forces in the vertical direction of the nodes on the contact boundary of the indenter.

The indentation hardness is defined as

$$H = \frac{P}{\pi a^2}. \tag{12}$$

During the finite element calculation, pile-up or sink-in is not imposed a priori, but a natural result of the indentation analysis. The comparison between contact depth, h_c, and the total depth, h_t, leads to sink-in or pile-up, i.e.,

$$\begin{aligned} &h_c < h_t \quad \text{sink-in}, \\ &h_c > h_t \quad \text{pile-up}. \end{aligned} \tag{13}$$

In the finite element calculation, we assume the glass substrate to be an elastic material and Al film an elastic-plastic one with a uniaxial stress–strain constitutive relation as,

$$\begin{cases} \sigma = E\varepsilon, & \sigma \leqslant \sigma_{\mathrm{Y}}, \\ \sigma = \sigma_{\mathrm{ref}}\varepsilon^{n}, & \sigma > \sigma_{\mathrm{Y}}, \end{cases} \tag{14}$$

where σ_{Y} is the yield stress of Al film, n the strain hardening exponent, and σ_{ref}, a reference stress which can be expressed by $\sigma_{\mathrm{ref}} = \sigma_{\mathrm{Y}}\,(E/\sigma_{\mathrm{Y}})^{n}$.

4.2. Identification of material parameters

Due to vanishing couple stresses on the outer boundaries, i.e., $m_{zz} = 0$, $m_{zr} = 0$, it can be proved easily that ω_i and m_{ij} are zero in the whole region, and the influence of l_{cs} has no significance in this kind of model. From the experimental results, we obtain the Young's modulus of glass substrate, $E_{\mathrm{glass}} = 88.5$ GPa. The Young's modulus of aluminum is close to that of glass, so that we take $E_{\mathrm{Al}} = 88.5$ GPa. Three parameters, i.e., the yield stress σ_y, power-law hardening exponent n, and the second intrinsic material length l are obtained by fitting the experimental load–depth curves. The interval $0.3t < h < 0.7t$ is chosen for fitting, where t denotes the thickness of the film. From Fig. 2, one can see that the dominative influence is caused by size effect at shallow depth; the substrate effect becomes stronger at larger depth, i.e., the indenter close to the interface. In the interval we choose to identify the film parameters, the role of both effects is almost equivalent. Thus we can take these plateaus to be good estimations of the true properties of films.

Virtual-Newton method (Dennis and Moré, 1977) is used to calibrate parameters, which is described in details as follows.

From the nano-indentation experimental results, we can obtain the corresponding load for each depth h, which is denoted as $P(h)$. For each chosen depth, h, we can also obtain a load, $P^{*}(h;\sigma,n,l)$ by FEM if the yield stress σ_{Y}, power-law hardening exponent n and the second intrinsic length l of films are given.

In order to find the three parameters of films, a group value of yield stress, power-law hardening exponent and the second intrinsic length are chosen initially, which can be denoted as σ_0, n_0 and l_0. Here, n_0 should be satisfied with $0 < n < 1$ and l_0 is chosen as $0 < l < 1$ μm inspired by Saha et al. (2001) and Chen et al. (2004a). The three parameters can be expressed by a vector $\boldsymbol{x}_0$, i.e., $\boldsymbol{x}_0 = \{\sigma_0, n_0, l_0\}$. We chose three values of depths h_1, h_2 and h_3 at the plateau of the hardness–depth curve, the corresponding values of loads $P(h_1)$, $P(h_2)$ and $P(h_3)$ can be found from the experimental data. For each selected depth, h_i $(i = 1, 2, 3)$, we can calculate a corresponding load $P^{*}(h_i, \boldsymbol{x}_0)$ by FEM. A vector function is introduced as follows

$$\boldsymbol{F}(\boldsymbol{x}_k) = \begin{pmatrix} f_1(\boldsymbol{x}_k) \\ f_2(\boldsymbol{x}_k) \\ f_3(\boldsymbol{x}_k) \end{pmatrix} = \begin{pmatrix} P^{*}(h_1,\boldsymbol{x}_k) - P(h_1) \\ P^{*}(h_2,\boldsymbol{x}_k) - P(h_2) \\ P^{*}(h_3,\boldsymbol{x}_k) - P(h_3) \end{pmatrix}, \tag{15}$$

The norm of function $\boldsymbol{F}(\boldsymbol{x}_k)$ can be expressed as

$$\|\boldsymbol{F}(\boldsymbol{x}_k)\| = \left[\sum_{i=1}^{3} f_i^{2}(\boldsymbol{x}_k)\right]^{1/2} = \left[\sum_{i=1}^{3}\left(P^{*}(h_i,\boldsymbol{x}_k) - P(h_i)\right)^{2}\right]^{1/2}. \tag{16}$$

with a given value of the tolerable limit $\varepsilon > 0$. If the norm of the function is less than the tolerable value, i.e., $\|\boldsymbol{F}(\boldsymbol{x}_0)\| < \varepsilon$, then $\{\sigma_0, n_0, l_0\}$ are the parameters we are searching for, otherwise iteration should be done. According to virtual-Newton method, a matrix will be introduced first, which is denoted as $\boldsymbol{B}$. Generally $\boldsymbol{B}$ is set as a unit matrix initially, here $\boldsymbol{B}_0 = \boldsymbol{I}_{3\times 3}$. According to matrix $\boldsymbol{B}_0$ and function $\boldsymbol{F}(\boldsymbol{x}_0)$, we can obtain another set of parameters, $\boldsymbol{x}_1 = \{\sigma_1, n_1, l_1\}$, by $\boldsymbol{x}_1 = \boldsymbol{x}_0 - \boldsymbol{B}_0^{-1}\boldsymbol{F}(\boldsymbol{x}_0)$. With the new parameters, we can calculate $\boldsymbol{F}(\boldsymbol{x}_1)$, if the norm of $\boldsymbol{F}(\boldsymbol{x}_1)$ is more than or equal to the tolerable value, i.e., $\|\boldsymbol{F}(\boldsymbol{x}_1)\| \geqslant \varepsilon$, iteration will continue following such two steps as

$$\boldsymbol{B}_{k+1} = \boldsymbol{B}_k + \frac{(\boldsymbol{y}_k - \boldsymbol{B}_k\boldsymbol{s}_k)\boldsymbol{s}_k^{\mathrm{T}}}{\langle \boldsymbol{s}_k, \boldsymbol{s}_k\rangle}, \quad \boldsymbol{x}_{k+2} = \boldsymbol{x}_{k+1} - \boldsymbol{B}_{k+1}^{-1}\,\boldsymbol{F}(\boldsymbol{x}_{k+1}), \quad (k = 1, 2, 3, \ldots) \tag{17}$$

where $\boldsymbol{s}_k = \boldsymbol{x}_{k+1} - \boldsymbol{x}_k = \Delta\boldsymbol{x}_k = \{\Delta\sigma_k, \Delta n_k, \Delta l_k\}$ denotes the increment of vector $\boldsymbol{x}_k$. $\boldsymbol{y}_k = \boldsymbol{F}(\boldsymbol{x}_{k+1}) - \boldsymbol{F}(\boldsymbol{x}_k)$ denotes the increment of vector $\boldsymbol{F}(\boldsymbol{x}_k)$, $\langle \mathbf{s}_k, \mathbf{s}_k \rangle$ the inner product of $\boldsymbol{s}_k$, i.e., $\langle \mathbf{s}_k, \mathbf{s}_k \rangle = \mathbf{s}_k^{\mathrm{T}} \cdot \mathbf{s}_k = \Delta\sigma_k^2 + \Delta n_k^2 + \Delta l_k^2$. Continuing the above steps, until a group of parameters $\boldsymbol{x}_{\mathrm{m}} = \{\sigma_{\mathrm{m}}, n_{\mathrm{m}}, l_{\mathrm{m}}\}$ is obtained, which satisfies $\|\boldsymbol{F}(\boldsymbol{x}_{\mathrm{m}})\| < \varepsilon$, then $\{\sigma_{\mathrm{m}}, n_{\mathrm{m}}, l_{\mathrm{m}}\}$ are the parameters we are searching for.

Finally, we obtain all the parameters for Al films with different thicknesses, which are shown in Table 1. From Table 1, one can see that the yield stress increases when the film thickness decreases, which is consistent with the experiment results (Venkatraman and Bravman, 1992; Hommel and Kraft, 2001; Schwaiger and Kraft, 2004). The power hardening exponent decreases with decreasing film thickness, which is consistent with our AFM measurements, i.e., grain size decreasing with decreasing film thickness. The intrinsic length scale l increases with a decreasing film thickness. The physical origin of different values of l for the same film material but with different film thicknesses can be explained by the theory proposed by Abu Al-Rub and Voyiadjis (2006) and MSG theory (Gao et al., 1999; Huang et al., 2000a). In Abu Al-Rub and Voyiadjis theory (2006), they found that l depends on not only the plastic strain level, the hardening level, but also the grain size, characteristic dimension of the specimen and hardening exponent. In MSG theory (Gao et al., 1999; Huang et al., 2000a), l has relation with the shear modulus, the Burgers vector, an empirical coefficient in the Taylor model and a reference stress, which has relation with the film thickness. Both mechanism-based theories prove that l should be different for the same material with different thickness. The experimental values of load and FEM results obtained by the fitting parameters are compared in Fig. 5.

4.3. Numerical results of nano-indentation hardness

After we obtain the parameters of Al films, indentation hardness can be further analyzed. Fig. 6(a)–(c) plot the indentation hardness predicted by both strain gradient plasticity and classical plasticity theories versus the normalized depth for Al films with different thicknesses on glass substrates, in which the same plastic work hardening exponent and yield stress are used for both theories in each case.

The size effect in nano- and micro-indentations is still an arguable problem, some researchers think that indenter tip curvature may be the main reason that leads to the increasing indentation hardness with decreasing indentation depth at the initial stage. During the present simulations with classical plasticity and strain

Table 1
Parameters of films obtained by fitting experimental data

Film thickness (nm)	Yield stress (MPa)	Power-law hardening exponent	Intrinsic length (μm)
52	310	0.02	0.8
245	154	0.05	0.6
851	123	0.10	0.5

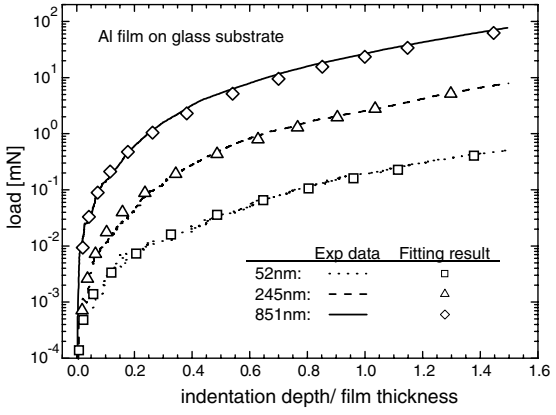

Fig. 5. Plots of load versus the normalized indentation depth for Al films on glass substrates with three different film thicknesses.

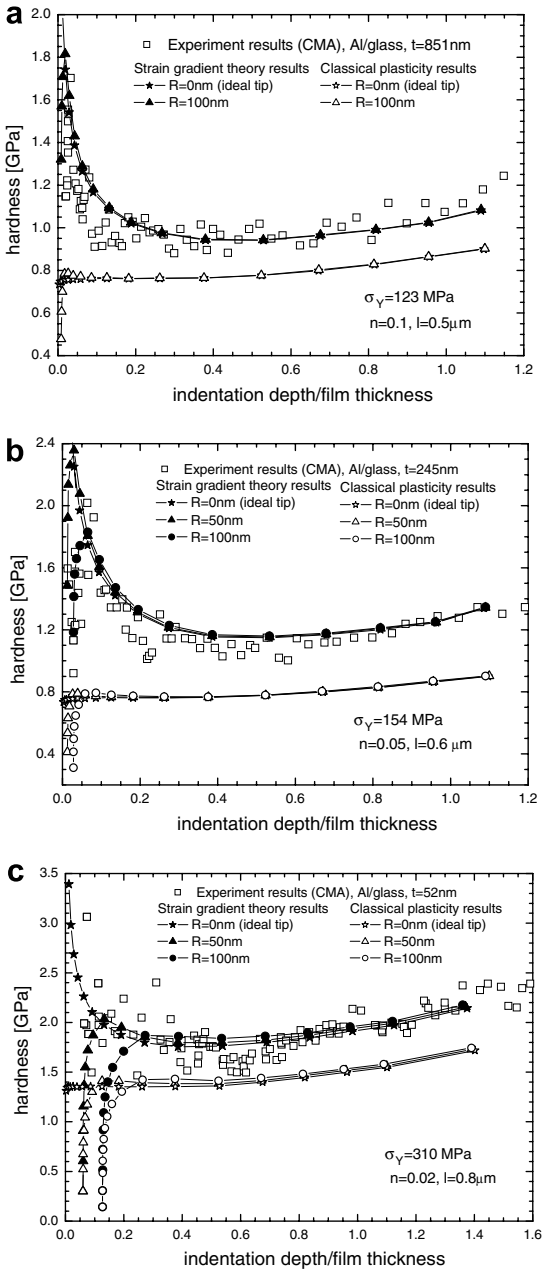

Fig. 6. Hardness versus the normalized indentation depth for Al–glass. Both the classical plasticity and strain gradient plasticity theories are used and each with both ideal and non-ideal indenters, respectively. (a) For 851 nm Al film on glass substrate; (b) for 245 nm Al film on glass substrate; (c) for 52 nm Al film on glass substrate.

gradient theories, both ideal sharp and spherically truncated indenters (non-ideal indenter tip) are considered, respectively. For the non-ideal indenter we take the radius of indenter tip as 50 and 100 nm (for 851 nm Al–glass system, the tip radius is set to be 100 nm only).

From Fig. 6(a)–(c), one can see that the results predicted by both ideal and non-ideal indenter tip with the classical plasticity theory are much smaller than the experimental data, especially in the initial region of indentation. The hardness with non-ideal indenter tip increases with an increasing indentation depth, then it keeps almost a constant except for the region with substrate effects. In the region that the indentation depth is com-

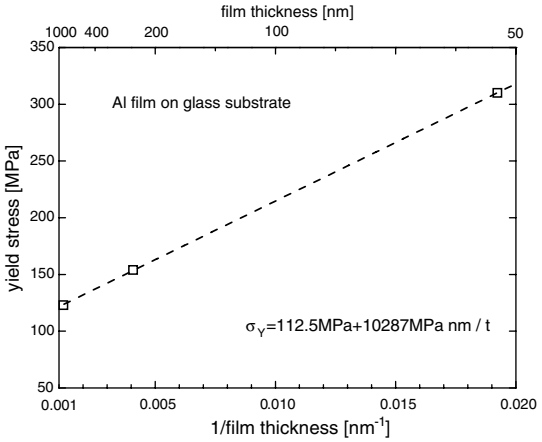

Fig. 7. Plot of yield stresses of films with different thicknesses versus the inverse of film thicknesses, which shows an almost linear relation.

parable to the film thickness, the predicted hardness by the classical plasticity theory is still much smaller than experimental results. The indenter curvature will influence the hardness only at the very shallow indentation depth and the effect will reduce along an increasing indentation depth. In the strain gradient theory, the calculated hardness with ideal indenter increases with decreasing depth of indentation at small depth. For the case with a non-ideal indenter, it decreases with decreasing depth of indentation at very small indentation depth, but the whole level of hardness is improved due to the existence of strain gradient effect and fits the experiment data quite well. In the region where the indentation depth is comparable to the film thickness, substrate effect becomes significant. The hardness predicted by the strain gradient theory in this region can still describe the experiment data well, which indicates that the strain gradient effect exists not only at the shallow indentation depth due to small size effects but also at the deep depth due to the films' compression between the indenter and the substrates.

One should note that a round indenter tip would result in an increasing hardness with an increasing indentation depth at the initial stage. The physical process responsible for such behavior is very clear and can be found in Johnson (1970) and Wei (2003a).

Finally, we plot the yield stresses as a function of the inverse of film thicknesses in Fig. 7. One can see that the relation between the yield stress and the inverse of film thickness keeps almost a linearity, which is in agreement with experimental studies (Hommel and Kraft, 2001; Schwaiger and Kraft, 2004).

5. Conclusions

In the present paper, film–substrate systems with three different sub-micrometer thicknesses of films are investigated using nano-indentation experiments and FEM simulations.

From experimental results, we find that the variation of indentation hardness with the indentation depth consists of three stages: at the shallow indentation depth, the indentation hardness decreases with an increasing indentation depth; then approximate constant indentation hardness follows; when the indenter is close to the film–substrate interface, the indentation hardness increases with an increasing indentation depth. Comparing systems with different film thicknesses, one can find that the hardness increases with a decreasing film thickness.

Parameters of Al film can be obtained using virtual-Newton method to fit the experimental load–depth curves. FEM simulations have been done with classical plasticity and strain gradient plasticity theories, as well as an ideal sharp indenter tip and a round indenter one, which shows that the classical plasticity can not explain the experimental data either with an ideal or a round indenter tip. However, the calculation results with strain gradient theory are consistent well with the experimental ones. The effects of indenter tip curvature are to reduce the hardness at the shallow indentation depth, not to improve the hardness and the strain gra-

dient effects should be included to explain the initial elevated hardness, which is consistent with the recent paper written by Huang et al. (2006).

Acknowledgement

The authors give their gratitude to the National Science Foundation of China (Nos. 10202023, 10272103, and 10672165) for support.

References

Abu Al-Rub, R., Voyiadjis, G.Z., 2004. Analytical and experimental determination of the material intrinsic length scale of strain gradient plasticity theory from micro- and nano-indentation experiments. Int. J. Plasticity 20, 1139–1182.
Abu Al-Rub, R., Voyiadjis, G.Z., 2006. A physically based gradient plasticity theory. Int. J. Plasticity 22, 654–684.
Acharya, A., Bassani, J.L., 2000. Lattice incompatibility and a general theory of crystal plasticity. J. Mech. Phys. Solids 48, 1565–1595.
Bassani, J., 2001. Incompatibility and a simple gradient theory of plasticity. J. Mech. Phys. Solids 49, 1983–1996.
Chen, S.H., Wang, T.C., 2000. A new hardening law for strain gradient plasticity. Acta Mater. 48, 3997–4005.
Chen, S.H., Wang, T.C., 2001. Strain gradient theory with couple stress for crystalline solids. Eur. J. Mech. A-Solids 20, 739–756.
Chen, S.H., Wang, T.C., 2002a. A new deformation theory for strain gradient effects. Int. J. Plasticity 18, 971–995.
Chen, S.H., Wang, T.C., 2002b. Finite element solutions for plane strain mode I crack with strain gradient effects. Int. J. Solids Struct. 39 (5), 1241–1257.
Chen, S.H., Wang, T.C., 2002c. Strain gradient effects in the particle-reinforced metal-matrix composites. Acta Mech. 157 (1–4), 113–127.
Chen, S.H., Wang, T.C., 2002d. Interface crack problems with strain gradient effects. Int. J. Fract. 117 (1), 25–37.
Chen, S.H., Liu, L., Wang, T.C., 2004a. Size dependent nano-indentation of a soft film on a hard substrate. Acta Mater. 52 (5), 1089–1095.
Chen, S.H., Tao, C.J., Wang, T.C., 2004b. A study of size-dependent micro-indentation. Acta Mech. 167 (1–2), 57–71.
Chen, S.H., Liu, L., Wang, T.C., 2005. Investigation of the mechanical properties of thin films by nano-indentation, considering the effects of thickness and different coating–substrate combinations. Surf. Coat. Technol. 191, 25–32.
Dennis, J.E., Moré, J.J., 1977. Quasi-Newton methods, motivation and theory. SIAM Rev. 19 (1), 46–89.
Duan, H.L., Wang, J., Huang, Z.P., Karihaloo, B.L., 2005. Size-dependent effective elastic constants of solids containing nano-inhomogeneities with interface stress. J. Mech. Phys. Solids 53, 1574–1596.
Fleck, N.A., Hutchinson, J.W., 1993. A phenomenological theory for strain gradient effects in plasticity. J. Mech. Phys. Solids 41, 1825–1857.
Fleck, N.A., Hutchinson, J.W., 1997. Strain gradient plasticity. In: Hutchinson, J.W., Wu, T.Y. (Eds.), Advances in Applied Mechanics, vol. 33. Academic Press, New York, pp. 295–361.
Fleck, N.A., Muller, G.M., Ashby, M.F., Hutchinson, J.W., 1994. Strain gradient plasticity: theory and experiment. Acta Metal. Mater. 42, 475–487.
Gao, H., Huang, Y., 2001. Taylor-based nonlocal theory of plasticity. Int. J. Solids Struct. 38, 2615–2637.
Gao, H., Huang, Y., Nix, W.D., Hutchinson, J.W., 1999. Mechanism-based strain gradient plasticity—I. Theory. J. Mech. Phys. Solids 47, 1239–1263.
Gerberich, W.W., Tymiak, N.I., Grunlan, J.C., Horstemeyer, M.F., Baskes, M.I., 2002. Interpretations of indentation size effects. J. Appl. Mech. 69, 433–442.
Gurtin, M.E., 2002. A gradient theory of single-crystal viscoplasticity that accounts for geometrically necessary dislocation. J. Mech. Phys. Solids 50, 5–32.
Gurtin, M.E., 2003. On a framework for small-deformation viscoplasticity: free energy, microforces, strain gradient. Int. J. Plasticity 19, 47–90.
Haque, M.A., Saif, M.T.A., 2003. Strain gradient effect in nanoscale thin films. Acta Mater. 51, 3053–3061.
Hommel, M., Kraft, O., 2001. Deformation behavior of thin copper films on deformable substrates. Acta Mater. 49, 3935–3947.
Horstemeyer, M.F., Baskes, M.I., Plimpton, S.J., 2001. Length scale and time scale effects on the plastic flow of FCC metals. Acta Mater. 49, 4363–4374.
Hu, G., Huang, Z., 2004. Micromechanics of nonlinear composites. Key Eng. Mater. 274–276, 35–42.
Huang, Y., Gao, H., Nix, W.D., Hutchinson, J.W., 2000a. Mechanism-based strain gradient plasticity—II. Analysis. J. Mech. Phys. Solids 48, 99–128.
Huang, Y., Xue, Z., Gao, H., Nix, W.D., Xia, Z.C., 2000b. A study of micro-indentation hardness tests by mechanism-based strain gradient plasticity. J. Mater. Res. 15, 1786–1796.
Huang, Y., Qu, S., Hwang, K.C., Li, M., Gao, H., 2004. A conventional theory of mechanism-based strain gradient plasticity. Int. J. Plasticity 20, 753–782.
Huang, Y., Zhang, F., Hwang, K.C., Nix, W.D., Pharr, G.M., Feng, G., 2006. A model of size effects in nano-indentation. J. Mech. Phys. Solids 54, 1668–1686.
Hwang, K.C., Jiang, H., Huang, Y., Gao, H., Hu, N., 2002. A finite deformation theory of strain gradient plasticity. J. Mech. Phys. Solids 50, 81–99.
Johnson, K.L., 1970. The correlation of indentation experiments. J. Mech. Phys. Solids 18, 115–126.

Joslin, D.L., Oliver, W.C., 1990. A new method for analyzing data from continuous depth-sensing micro-indentation tests. J. Mater. Res. 5, 123–126.
Kreuzer, H.G.M., Pippan, R., 2005. Discrete dislocation simulation of nano-indentation: the influence of obstacles and a limited number of dislocation sources. Philo. Magazine 85, 3301–3319.
Liu, X., Hu, G., 2005. A continuum micromechanical theory of overall plasticity for particulate composites including particle size effect. Int. J. Plasticity 21, 777–799.
Lloyd, D.J., 1994. Particle-reinforced aluminum and magnesium matrix composite. Int. Mater. Rev. 39, 1–23.
Ma, Q., Clarke, D.R., 1995. Size dependent hardness of silver single crystals. J. Mater. Res. 10, 853–863.
McElhaney, K.W., Vlassak, J.J., Nix, W.D., 1998. Determination of indenter tip geometry and indentation contact area for depth-sensing indentation experiments. J. Mater. Res. 13, 1300–1306.
Nix, W.D., 1989. Mechanical properties of tin films. Metal. Trans. 20A, 2217–2245.
Nix, W.D., Gao, H., 1998. Indentation size effects in crystalline materials: a law for strain gradient plasticity. J. Mech. Phys. Solids 46, 411–425.
Oliver, W.C., Pharr, G.M., 1992. An improved technique for determining hardness and elastic modulus using load and displacement sensing indentation experiments. J. Mater. Res. 7 (6), 1564–1583.
Poole, W.J., Ashby, M.F., Fleck, N.A., 1996. Micro-hardness of annealed and work-hardened copper polycrystals. Scripta Mater. 34, 559–564.
Pucha, R.V., Ramakrishna, G., Mahalingam, S., Sitaraman, S.K., 2004. Modeling spatial strain gradient effects in thermo-mechanical fatigue of copper microstructures. Int. J. Fatigue 26, 947–957.
Qu, S., Huang, Y., Nix, W.D., Jiang, H., Zhang, F., Hwang, K.C., 2004. Indenter tip radius effect on the Nix–Gao relation in micro- and nano-indentation hardness experiments. J. Mater. Res. 19, 3423–3434.
Qu, S., Huang, Y., Pharr, G.M., Hwang, K.C., 2006. The indentation size effect in the spherical indentation of iridium: A study via the conventional theory of mechanism-based strain gradient plasticity. Int. J. Plasticity 22, 1265–1286.
Saha, R., Nix, W.D., 2002. Effects of the substrate on the determination of thin film mechanical properties by nano-indentation. Acta Mater. 50, 23–38.
Saha, R., Xue, Z., Huang, Y., Nix, W.D., 2001. Indentation of a soft metal film on a hard substrate: strain gradient hardening effects. J. Mech. Phys. Solids 49, 1997–2014.
Schwaiger, R., Kraft, O., 2004. Analyzing the mechanical behavior of thin films using nano-indentation, cantilever microbeam deflection, and finite element modeling. J. Mater. Res. 19 (1), 315–324.
Shrotriya, P., Allameh, S.M., Lou, J., Buchheit, T., Soboyejo, W.O., 2003. On the measurement of the plasticity length-scale parameter in LIGA nickel foils. Mech. Mater. 35, 233–243.
Smyshlyaev, V.P., Fleck, N.A., 1996. The role of strain gradients in the grain size effect for polycrystals. J. Mech. Phys. Solids 44, 465–495.
Stelmashenko, N.A., Walls, A.G., Brwon, L.M., Milman, Y.V., 1993. Micro-indentation on W and Mo oriented single crystals: an STM study. Acta Metal. Mater. 41, 2855–2865.
Stolken, J.S., Evans, A.G., 1998. A microbend test method for measuring the plasticity length scale. Acta Mater. 46, 5109–5115.
Suresh, S., Nieh, T.G., Choi, B.W., 1999. Nano-indentation of cooper thin films on silicon substrates. Scripta Mater. 41, 951–957.
Swaddiwudhipong, S., Poh, L.H., Hua, J., Liu, Z.S., Tho, K.K., 2005. Modeling nano-indentation tests of glass polymers using finite elements with strain gradient plasticity. Mater. Sci. Eng. A 404, 179–187.
Swaddiwudhipong, S., Hua, J., Tho, K.K., Liu, Z.S., 2006a. Finite element modeling for materials with size effect. Model. Simul. Mater. Sci. Eng. 14, 1127–1137.
Swaddiwudhipong, S., Tho, K.K., Hua, J., Liu, Z.S., 2006b. Mechanism-based strain gradient plasticity in C0 axisymmetric element. Int. J. Solids Struct. 43, 1117–1130.
Swadener, J.G., Taljat, B., Pharr, G.M., 2001. Measurement of residual stress by load and depth sensing indentation with spherical indenters. J. Mater. Res. 16, 2091–2102.
Swadener, J.G., George, E.P., Pharr, G.M., 2002. The correlation of the indentation size effect measured with indenters of various shapes. J. Mech. Phys. Solids 50, 681–694.
Venkatraman, R., Bravman, J.C., 1992. Separation of film thickness and grain-boundary strengthening effects in al thin-films on Si. J. Mater. Res. 7, 2040–2048.
Voyiadjis, G.Z., Abu Al-Rub, R.K., 2005. Gradient plasticity theory with a variable length scale parameter. Int. J. Solids Struct. 42, 3998–4029.
Wei, Y., 2003a. Hardness solution form for elastic-plastic material considering the indenter tip curvature effect. Acta Mech. Sin. 35, 509–512 (in Chinese).
Wei, Y., Hutchinson, J.W., 1997. Steady-state crack growth and work of fracture for solids characterized by strain gradient plasticity. J. Mech. Phys. Solids 45, 1253–1273.
Wei, Y., Hutchinson, J.W., 2003b. Hardness trends in micro scale indentation. J. Mech. Phys. Solids 51, 2037–2056.
Wei, Y., Wang, X., Zhao, M., Cheng, C.M., Bai, Y., 2003c. Size effect and geometrical effect of solids in micro-indentation test. Acta Mech. Sin. 19, 59–70.
Xue, Z., Huang, Y., Hwang, K.C., Li, M., 2002. The influence of indenter tip radius on the micro-indentation hardness. J. Eng. Mater. Tech. 124, 371–379.